Role of washing process in the improvement of surface properties of porous geopolymers

Lahcen Bouna (bounalahcen@gmail.com)
Université Ibn Zohr
Youssef Ettahiri
Université Ibn Zohr
Antoine Elimbi
Université de Yaoundé I
Abdeljalil Benlhachemi
Université Ibn Zohr
Martin Cyr
Université de Toulouse

Research Article

Keywords: Geopolymers, washing process, porosity, specific surface area, improvement

Posted Date: October 10th, 2022

DOI: https://doi.org/10.21203/rs.3.rs-2123923/v1

Additional Declarations: No competing interests reported.

Version of Record: A version of this preprint was published at Journal of Porous Materials on November 21st, 2023. See the published version at https://doi.org/10.1007/s10934-023-01533-0.

Abstract

This study investigates the importance of washing process in the quantitative improvement of both porosity and specific surface area of geopolymer. To this end, geopolymer was synthesized using natural kaolinite clay via alkaline activation. Depending on both unwashed and washed geopolymers, the following characterization techniques were achieved: X-ray Diffraction (XRD), Fourier Transform Infrared (FTIR) spectroscopy, Thermal Gravimetric Analysis (TGA), specific surface area, pore distribution, pore volume and Scanning Electron Microscopy (SEM). After the washing process, both specific surface area (S_{BET}) and pore volume (Vp) of geopolymers have increased considerably: S_{BET} = 0.59 m^2/g and Vp = 0.001 cm^3/g (unwashed) versus S_{BET} = 78.80 m^2/g and Vp = 0.104 cm^3/g (washed) respectively. Hence, the washing process allows increasing of the surface reactivity of geopolymers through the elimination among others of excess of unreacted alkaline solution which is responsible of the efflorescence.

1- Introduction

Geopolymers have taken great importance in recent years as efficient and economical adsorbents for the treatment of effluents containing various organic and inorganic pollutants [1–4]. However, details in the literature concerning porosity and specific surface area of those materials are rarely found, although these properties are of prime importance for this usage. Rouyer et al., 2017, Singhal et al., 2017, Koshy et al., 2019, and Tome et al., 2021 investigated the determination of specific surface area and porosity of geopolymers [2, 5–7]. However, the latter authors did not explain the role and the importance of the washing process. Cheng et al., 2012 showed that the specific surface area of metakaolin-based geopolymer increases after successive washings with distilled water, causing the removal of unreacted excess alkali ingredients and other debris [22]. In the studies done by Duxson et al., 2007 and Davidovits, 2008, the alkaline activation solution that was used helped to form a homogeneous gel necessary to get geopolymers with remarkable chemical and mechanical properties [8, 9]. Many studies demonstrated that the increase of both curing temperature and water /solid mass ratio increases the porosity of geopolymers [23, 24]. Other researchers used additional agents favoring the formation of porous geopolymers through the incorporation of surfactants, natural organic compound, H_2O_2, etc. [1, 2, 25]. The present work is focused specially on studying and detailing the role of washing process in the improvement of properties of porous geopolymers such as BET specific surface area and BJH pores volume. We have chosen the water to solid mass ratio and the curing temperature of geopolymerization that favoring the pores creation in our geopolymer. Presently, in order to eliminate the excess of unreacted alkali activator in the pores and on the surface of the synthesized products, the synthesized geopolymers were submitted to the washing process. Also, the following characterization techniques were performed on the geopolymer: X ray Diffraction (XRD), Fourier Transform Infrared (FTIR) spectroscopy, Thermal Gravimetric Analysis (TGA) in the range of 25-1000°C and Scanning Electron Microscopy (SEM). The determination of surface specific area and pore volume of geopolymers was carried out as well thanks to the BET method.

2- Material And Methods

a. Synthesis of geopolymers

The precursor used to prepare the geopolymer was a natural kaolinite rich clay whose characteristics are found in Bouna et al., 2020 [11]. The metakaolin was obtained by calcination of the natural kaolinite clay at 800 °C for 8h in air thanks to an electric muffle furnace, type Lenton FURNACES. To get the geopolymer, 2g of powder of metakaolin were added to alkaline activating solution whose composition was as follows: 14.5 ml of distilled water in which were respectively dissolved 1.08g of silicon dioxide and 1.08g of pellet of sodium hydroxide. This led to alkaline activating solution with H_2O/Na_2O = 15, Si/Al = 2 and Na/Al = 1.5 respectively [10]. The mixture was stirred for 30 min and the obtained paste was oven-dried at 70°C for 24 hours in order to get a solid which was devised into two parts. One part was not washed and was denoted as UW-GP. The other part which was initially washed for several times via distilled water followed of drying was referenced as W-GP. Then after, both UW-GP and W-GP solids were crushed in order to get geopolymer powders.

b. Characterization methods

The metakaolin and the geopolymer were characterized by X-ray Diffraction (XRD) using Bruker D8 Advance Twin diffractometer equipped with a LYNXEYE XE-T linear detector, $CuK\alpha_1$ (λ= 1.5418 A°), time of recording 0.3s, step scanning of 0.05° in the interval (2θ) of 5-60°. Fourier Transform Infra-Red (FTIR) spectroscopy was carried out in the range of 400-4000 cm^{-1} using the IRAffinity-1S Shimadzu spectrophotometer. The samples were also characterized by Thermal Gravimetric Analysis (TGA) by a Q500 TA device. To this end, powder of the geopolymer was heated in air from room temperature to 1000°C at heating and cooling rates of 10 °C/min respectively. Specific surface area of the dried sample was determined using the Brunauer– Emmett–Teller (BET) method by applying the BET equation for the relative pressure range $0.05<P/P_0<0.30$ from these isotherms [12]. Nitrogen adsorption isotherms at 77 K were utilized using an adsorption analyzer from Micromeritics (3-Flex 4.01version). Total pore volume (V_T) of pores width less than 198.8 Å was determined from the volume of adsorbed nitrogen at a relative pressure of 0.89. The mesopore size distribution was determined by Barrett–Joyner–Halenda (BJH) method assuming a cylindrical pore model [13]. Prior to the N_2 adsorption-desorption measurements, the specimens were out-gassed at 200 ºC for 12 h. Scanning Electron Microscopy (SEM) analysis was used to examine the microstructure of specimens. The device used was a Jeol TSM-IT100 operating at 20 KeV, coupled with an Energy Dispersive X-ray Spectroscopy (EDS) analyzer, allowing determining the local elemental compositions in different zones.

c. Adsorption tests

The adsorption tests were performed using a methylene blue MB dye. It was chosen to determine the adsorption capacity of washed and unwashed samples. The initial concentration C_0 of MB dye was fixed at 200 mg/L. The starting pH was 7.1. The experiments were carried out at room temperature into closed

vials and then stirred for 24 h. Then after, the suspensions were centrifuged for analyzing the supernatant using a VIS-7220G visible spectrophotometer. The amount of MB adsorbed at equilibrium time per gram of adsorbent (q_e, mg/g), was evaluated according to equation [32]:

$$q_e = \frac{(C_0 - Ce)V}{m}$$

where C_0 (mg L^{-1}) and C (mg $^{L-1}$) are MB dye concentrations at the initial and equilibrium time, respectively. m is the mass of adsorbent (g) and V is the solution volume (mL).

3- Results And Discussion

a. XRD analyzes

Fig.1 shows the XRD diffractograms of metakaolin, unwashed (UW-GP) and washed (W-GP) geopolymers. The diffractogram of metakaolin shows the presence of minerals such as quartz and potassium aluminum silicate $K(Si_3Al)(Al_2)O_{11}$ (PDF: 046–0741) as a result of calcination of muscovite [10]. The diffractogram of the UW-GP shows a hump in the angular range of 20 to 35°, confirming the formation of geopolymer gel [1,2,14]. There are also the characteristic peaks of sodium carbonate monohydrate $Na_2CO_3.H_2O$ (PDF: 070-2148) that was formed under the effect of atmospheric CO_2 [6]. The XRD diffractogram of W-GP shows the disappearance of sodium carbonate monohydratepeaks after successive washings. Furthermore, the hump expressing the amorphous geopolymer gel is slightly attenuated in the diffractogram of W-GP while the peak intensities of associated minerals have increased, which shows structural reorganization after both the washing process and the removal of alkaline solution excess.

b. Infrared spectroscopy analyzes

The FTIR spectra of metakaolin, UW-GP and W-GP are shown in Fig. 2. The metakaolin spectrum exhibits the different vibrations of Si-O bond (470, 534, 796 and 1038 cm^{-1} respectively) and Al-O vibration bond (around 692 cm^{-1}) that correlate with the structure of metakaolin, quartz and potassium aluminum silicate phases [10]. The spectrum of UW-GP shows a wide vibration band in the range 3100-3700 cm^{-1} characterizing the amorphous geopolymer gel [1,2]. The band that appears around 1670 cm^{-1} is due to the bending vibration of water molecules adsorbed on the surface and in the pores of geopolymer [2]. The vibration bands around 867, 1463 and 2900 cm^{-1} refer to sodium carbonates monohydrate that were already detected by XRD analysis. These last three bands have completely disappeared in the W-GP as a result of successive washings under distilled water. The band between 660 and 740 cm^{-1} with maximum intensity around 692 cm^{-1} appears clearer in W-GP sample and corresponds to symmetric and

asymmetric Si-O-T (T = Si or Al) vibrations in SiO_4 or AlO_4 tetrahedral of the amorphous gel of geopolymer [1,6,15]. Finally, the shifting position of the asymmetric stretching Si-O-Si bond to lower wavenumber respectively for UW-GP and W-GP (1026 cm^{-1}) as compared with metakaolin (1038 cm^{-1}) indicates the formation of Si-O amorphous bonds, characterizing the geopolymer [1,16].

c. TGA analyzes

Fig. 3 shows the thermograms of UW-GP and W-GP respectively. The thermogram of UW-GP shows greater total mass loss as compared to that of W-GP. This mass loss is due to the intervention of several phenomena namely: departure of adsorbed water on the surface of geopolymer (<150 °C) [17,18], departure of water of sodium carbonate monohydrate which was detected also by XRD and FTIR analyses (110-180 °C) [19] and this mass loss is higher for UW-GP than for W-GP; removal of water from both excess of unreacted alkali solution [18] and hydrated aluminosilicate around 180-400 °C [14], this mass loss being more important for UW-GP than for W-GP. Indeed, the study done by Chen et al., 2021 shows that the mass loss of geopolymers increases with increasing alkaline solution concentration used in the synthesis process [19]. Elimination of bound water generated by silanol and aluminol groups (Al-OH or Si-OH) on the surface of the material is generally between 400 and 540 °C [19]. However, any mass loss in the range 540-860 °C was observed for both samples (UW-GP and W-GP), indicating the good preparation of metakaolin used for geopolymerization. Finally, a weak mass loss starting at 860° C showed only for UW-GP corresponds to the formation of CO_2 as a result of thermal decomposition of sodium carbonate monohydrate, which was also detected by XRD and FTIR analyzes [19,20].

d. BET specific surface area and BJH mesopore distributions

Fig. 4 presents the adsorption-desorption isotherm curves whereas Fig. 5 shows the mesopore width distributions obtained by BJH method for UW-GP and W-GP respectively. On the one hand, for UW-GP, the values of specific surface area and porevolume are very low. On the other hand, for W-GP, there is a true isotherm IV type with H3 hysteresis loops according to the classification of the International Union of Pure and Applied Chemistry (IUPAC), indicating that there were slit-like pores in the washed material. Both specific surface area (S_{BET} = 78.8 m^2/g) and pore volume (Vp = 0.104 cm^3/g) in this sample have been significantly increased after successive washings. Similar isotherm and hysteresis types were obtained by Singhal et al., 2017 [2]. This result shows that the washing process allows to empty the pores and to free the surface of geopolymer from excess of unreacted alkali activation solution and to remove sodium carbonate monohydrate formed during the synthesis under the action of atmospheric CO_2 air (efflorescence). The mechanism of washing process and the interaction of N_2 molecules into washed and unwashed geopolymers surfaces was described in Fig. 5. The pore distribution size curve of W-GP shows homogeneous mesopores of around 40 A° width (Fig.6).

Table 1 presents the bibliographic data concerning the washed and the unwashed geopolymers, summarizing the values obtained from BET specific surface area, BJH pore volume and the amount of different chemical entities adsorbed by the geopolymers samples. One the one hand, it clearly appears

that the unwashed geopolymers have both low specific surface area and pore volume as compared to the washed ones. On the other hand, for our study the unwashed geopolymers don't have a significant effect on adsorption capacity because the value retained in methylene blue by unwashed sample (52.2 mg/g) was only 6% improved after washing process (55.6 mg/g). The literature data presented in table 1 show that both washed and unwashed geopolymers have high adsorption capacity for retaining a different heavy metals and organic dyes. This result indicates that the improvement of specific surface area and pore volume of geopolymers specimens is not a necessary condition for increasing the adsorption capacity. This is strongly due to the releasing the surfaces and pores of unwashed sample in the unreacted alkaline excess under effect of the medium water during adsorption processes.

Table 1

Characteristics of unwashed and with washing process geopolymers.

Geopolymer sample	Washing the sample	Adsorbate	Amount adsorbed (mg/ g)	S_{BET} (m^2 /g)	V_{BJH} (cm^3/g)	Ref.
Fly ash based geopolymer	Yes	Sodium dodecyl benzene sulfonate SDBS surfactant	743.70	59.5	0.133	Ali Siyal et al., 2021 [26]
Geopolymer based metakaolin	No	methylene blue	43.48	n.r.	n.r.	El Alouani et al., 2019 [27]
Magnetic geopolymer based bentonite	No	Cu(II), Pb(II), Ni(II), Cd(II), and Hg(II)	300 – 550	1.13	0.004	Maleki et al., 2019 [28]
Porous inorganic polymer spheres based metakaolin	Yes	Cu(II), Pb(II) and Ca(II)	35.5, 45.6 and 24.0	53.95	n.r.	Tang et al., 2015 [29]
Geopolymer based metakaolin	No	n.r.	n.r.	50.9	n.r.	Cheng et al., 2012 [22]
	Yes	Pb(II), Cu(II), Cr(III) and Cd(II)	10 – 100	65.7	n.r.	
Mesoporous geopolymer based metakaolin and rice husk ash	Yes	methyl violet 10B	276.9	62	0.36	Barbosa et al., 2018 [1]
Nanoporous geopolymer based metakaolin	Yes	Cu(II)	40	216	0.22	Singhal et al., 2017 [2]
Geopolymer based LD slag	Yes	Ni (II)	85.29	30.84	0.091	Sarkar et al., 2017 [30]
Geopolymer based metakaolin	No	Pb(II), Cu(II), Cd(II), Ni(II), Zn(II) and Cs(I)	5 – 57	3.3	n.r.	López et al., 2014 [31]
Geopolymers based industrial by-products	No	n.r.	n.r.	5 – 25	n.r.	Koshy et al., 2019 [6]
Geopolymer based natural kaolinite	No	methylene blue	52.2	0.59	0.001	This study
	Yes	methylene blue	55.6	78.8	0.104	

n.r. = not reported

e. SEM analyzes

The morphology of metakaolin, UW-GP and W-GP are showed respectively in Fig. 7. Also, Table 2 gives the atomic fractions, obtained by EDS analysis, as well as the Si/Al and Na/Al formulation ratios of the three samples. The SEM image of Fig.7-a confirms the microstructure of metakaolin [2,14], while the SEM image of Fig.7-b (UW-GP) shows an amorphous phase, characteristic of geopolymer with high homogeneity on the surface along with very low porosity between particles. In addition, the SEM images of Fig.7-(c,d) (W-GP) show the microstructure of amorphous geopolymer with great porosity between the particles. Such almost porous morphology was already obtained by Wang et al., 2005 and Selmani et al., 2017 and Koshy et al., 2019 [6,14,21]. The formulation ratios Si/Al and Na/Al have increased for UW-GP (Table 2) as compare to those of the metakaolin, these probably being due to SiO_2 and NaOH used for preparing the alkaline activation solution. Conversely, both Si / Al and Na / Al ratios have significantly decreased in W-GP as a result of removal of sodium carbonate monohydrate and departure of large part of water-soluble products of unreacted alkaline solution. This result highlights and consolidates those previously obtained, which confirms the fact that the washing process allows both removal of excess of unreacted alkaline solution and sodium carbonate monohydrate that occupy the surface and the pores of unwashed geopolymer.

Table 2

Elementary compositions of metakaolin, UW-GP and W-GP obtained by EDS.

	% atomic							Formulation ratio	
Sample	Si	Al	K	Na	Fe	Mg	Ti	Si/Al	Na/Al
Metakaolin	53.6	36.4	7.1	1.3	1.5	0.0	0.1	1.47	0.03
UW-GP	43.8	17.7	1.8	35.8	0.8	0.0	0.0	2.47	2.02
W-GP	54.6	27.9	5.6	11.0	0.0	0.0	0.8	1.95	0.39

4- Conclusion

The washing process is an important step for a careful and quantitative improvement of porosity and specific surface area of geopolymers. Because this allows emptying the pores of and to free the surface of geopolymer by removing both unreacted matter and excess of alkaline activation solution. The washing process also allows removal of sodium carbonate monohydrate formed under the effect of atmospheric carbon dioxide of air (efflorescence). Under the washing process of geopolymer, both specific surface area and pore volume have increased considerably: S_{BET} = 0.59 m^2/g and Vp = 0.001 cm^3/g (unwashed) versus S_{BET} = 78.8 m^2/g and Vp = 0.104 cm^3/g (washed). Moreover, the improvement

of specific surface area and pore volume of geopolymers specimens is not a necessary condition for increasing the adsorption capacity.

References

1. T.R. Barbosa, E.L. Foletto, G.L. Dotto, S.L. Jahn, Ceramics International. 44, 416–423 (2018)
2. A. Singhal, B.P. Gangwar, J.M. Gayathry, Applied Clay Science. 150, 106–114 (2017)
3. S.A. Rasaki, Z. Bingxue, R. Guarecuco, T. Thomas, Y. Minghui, Journal of Cleaner Production. 213, 42–58 (2019)
4. A. Maleki, Z. Hajizadeh, A. Sharifi, Z. Emdadi, Journal of Cleaner Production. 215, 1233–1245 (2019)
5. J. Rouyer, V. Benavent, F. Frizon, A. Poulesquen, Materials Letters. 207, 121–124 (2017)
6. N. Koshy, K. Dondrob, L. Hu, Q. Wen, J.N. Meegoda, Constr. Build Mater. 206, 287–296 (2019)
7. S. Tome, D.T. Hermann, V.O. Shikuku, S. Otieno, Ceramics International. 47, 20965–20973 (2021)
8. P. Duxson, J.L. Provis, G.C. Lukey, J.S.J. van Deventer, Cem. Concr. Res. 37, 1590–1597 (2007)
9. J. Davidovits, Chemistry and Applications, Geopolymer Institute. Second ed. Saint-Quentin, France (2008)
10. L. Bouna, A. Ait El Fakir, A. Benlhachemi, K. Draoui, M. Ezahri, B. Bakiz, S. Villain, F. Guinneton, N. Elalem, Applied Clay Science. 196, 105764 (2020)
11. L. Bouna, A. Ait El Fakir, A. Benlhachemi, K. Draoui, S. Villain, F. Guinneton, Materials Today: Proceedings. 22, 22–27 (2020)
12. S. Brunauer, P.H. Emmet, E. Teller, Journal of American Chemical Society, 60, 309–319 (1938)
13. E.P. Barrett, L.G. Joyner, P.P. Halenda, J. Am. Chem. Soc. 73, 373–380 (1951)
14. S. Selmani, A. Sdiri, S. Bouaziz, E. Joussein, S. Rossignol, Applied Clay Science. 146, 457–467 (2017)
15. N.K. Lee, H.R. Khalid, H.K. Lee, Microporous Mesoporous Mater. 229, 22–30 (2016)
16. Z. Zhang, H. Wang, X. Yao, Y. Zhu, Cem. Concr. Compos. 34, 709–715 (2012)
17. P. Duxson, G.C. Lukey, J.S.J. van Deventer, J. Non. Cryst. Solids. 352, 5541–5555 (2006)
18. E. Prud'Homme, P. Michaud, E. Joussein, J.M. Clacens, S. Arii-Clacens, I. Sobrados, C. Peyratout, A. Smith, J. Sanz, S. Rossignol, J. Non-Cryst. Solids. 357, 3637–3647 (2011)
19. K. Chen, W.T. Lin, W. Liu, Advanced Powder Technology. 32, 2929–2939 (2021)
20. J.W. Kim, Y.D. Lee, H.G. Lee, ISIJ Int. 41, 116–123 (2001)
21. H. Wang, H. Li, F. Yan, Colloids and Surfaces A: Physicochem. Eng. Aspects. 268, 1–6 (2005)
22. T.W. Cheng, M.L. Lee, M.S. Ko, T.H. Ueng, S.F. Yang, Applied Clay Science. 56, 90–96 (2012)
23. R. Pouhet, M. Cyr, R. Bucher, Constr. Build. Mater. 201, 421–429 (2019)
24. V. Benavent, F. Frizon, A. Poulesquen. J. Appl. Crystallogr. 49 (6), 2116–2128 (2016)
25. S. Petlitckaia, A. Poulesquen, Ceramics International. 45, 1322–1330 (2019)

26. A.A. Siyal, M.S. Shamsuddin, S.K. Khahro, A. Low, M. Ayoub, Journal of Environmental Chemical Engineering. 9, 104949 (2021)
27. M. El Alouani, S. Alehyen, M. El Achouri, M. Taibi, Journal of Chemistry. 4212901 (2019)
28. A. Maleki, Z. Hajizadeh, V. Sharifi, Z. Emdadi, Journal of Cleaner Production. 215, 1233–1245 (2019)
29. Q. Tang, Y. Ge, K. Wang, Y. He, X. Cui, Materials and Design. 88, 1244–1249 (2015)
30. C. Sarkar, J.K. Basu, A.N. Samanta, J. Water Process Eng. 17, 237–244 (2017)
31. F.J. López, S. Sugita, M. Tagaya, T. Kobayashi, J. Mater. Sci. Chem. Eng. 2, 16–27 (2014)
32. P.T. Hang, G.W. Brindley, Clays Clay Miner. 18, 203–212 (1970)

Figures

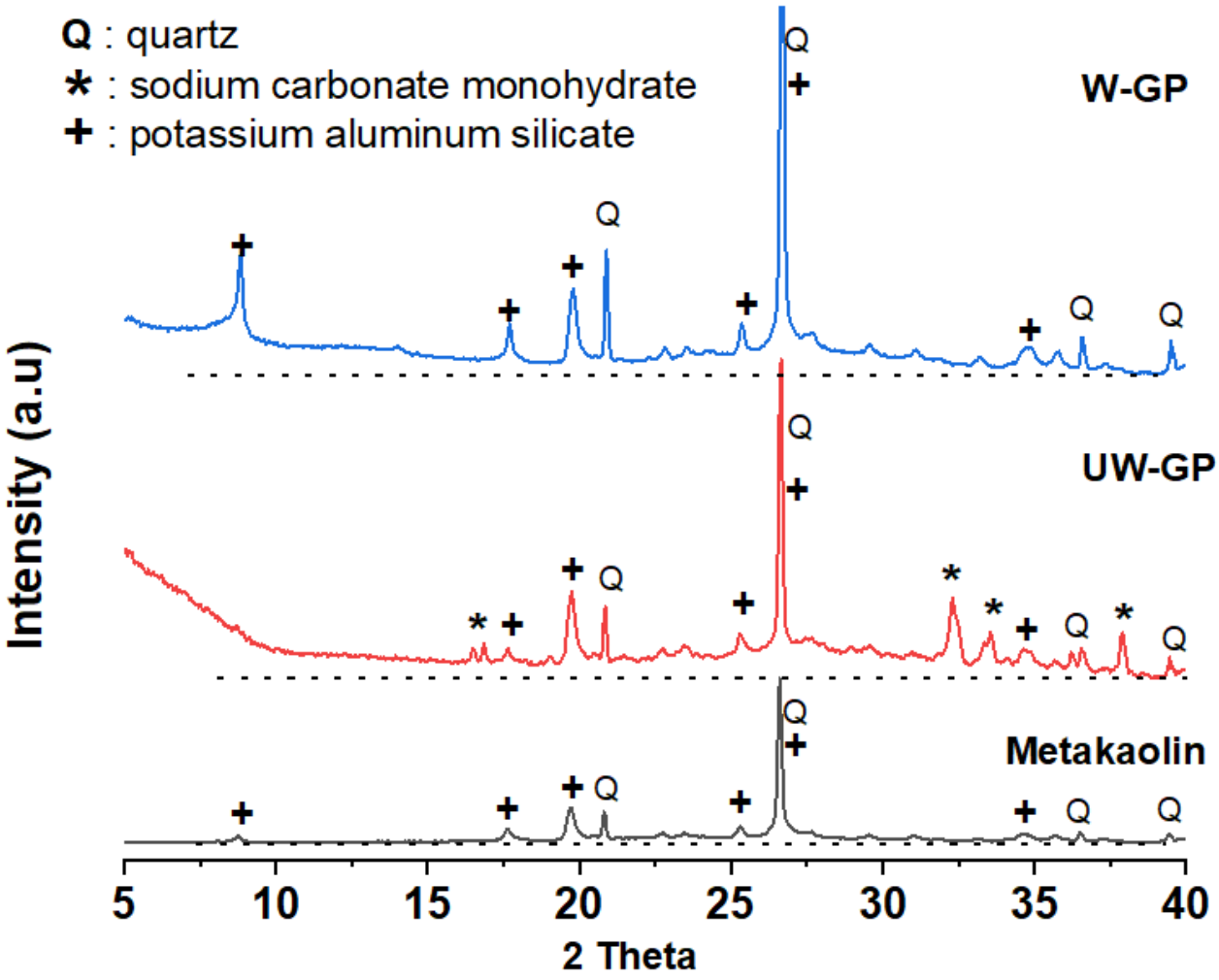

Figure 1

X-ray patterns of metakaolin, UW-GP and W-GP.

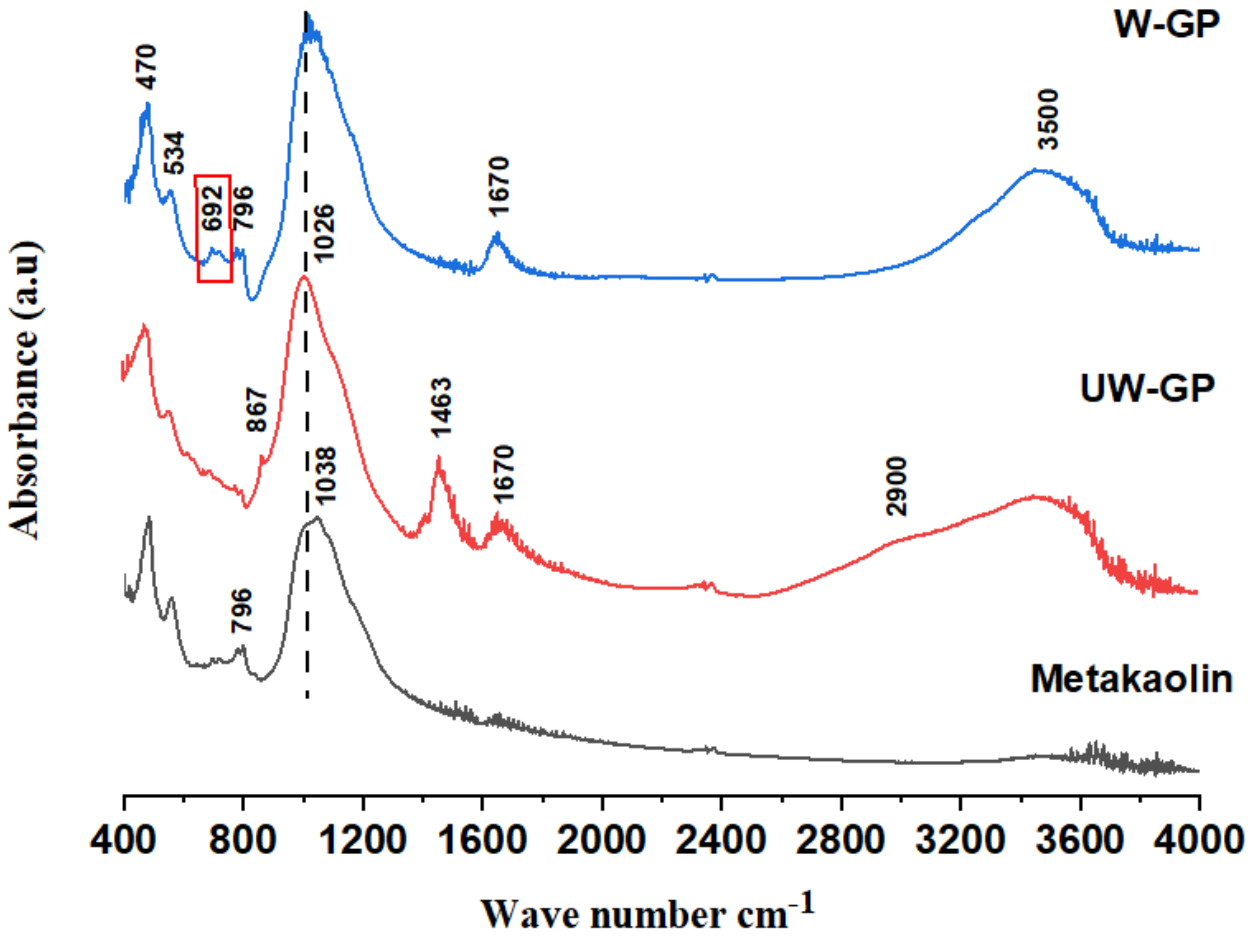

Figure 2

FTIR spectra of metakaolin and UW-GP and W-GP.

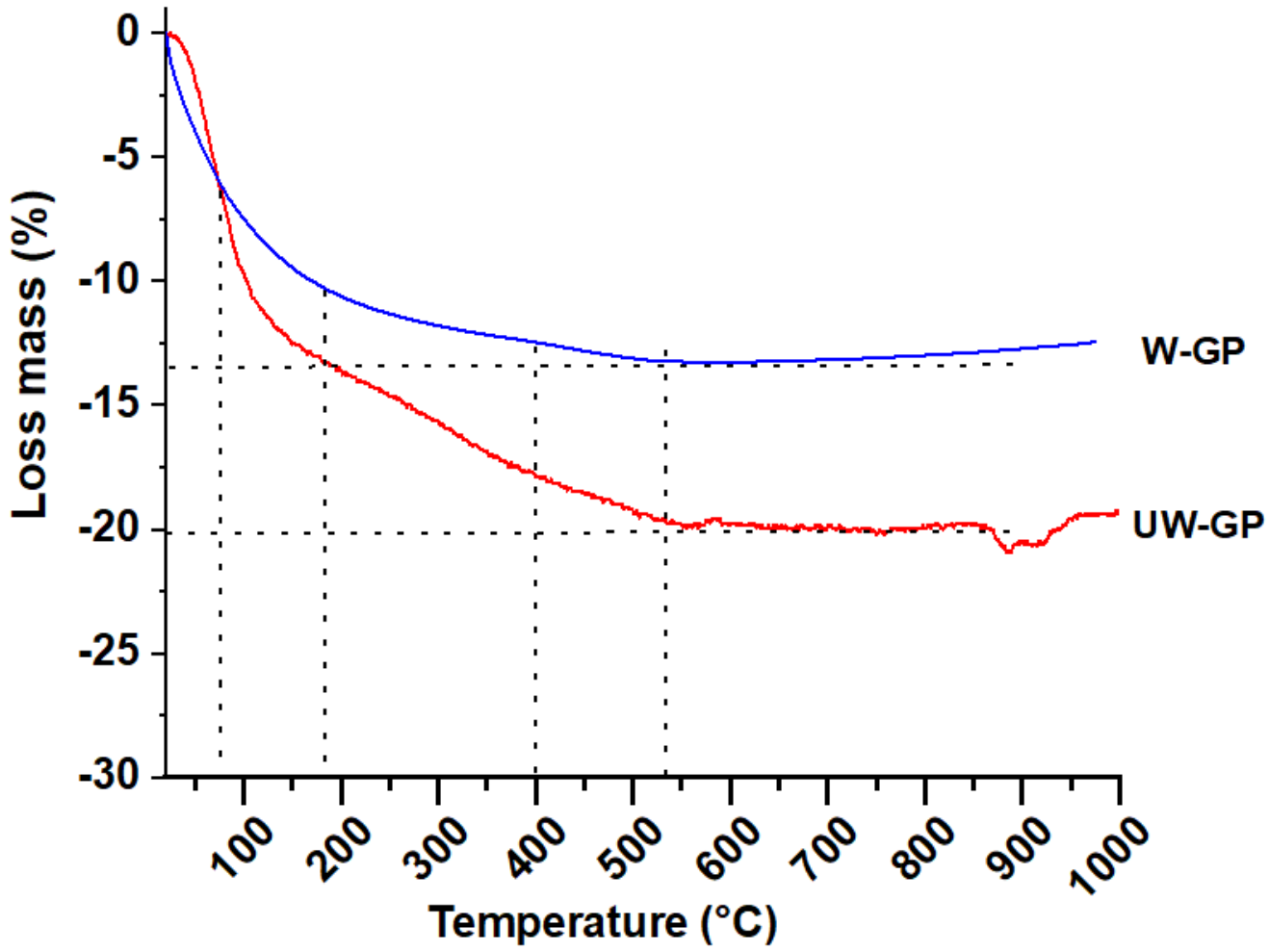

Figure 3

TGA thermal analyses of metakaolin and UW-GP and W-GP

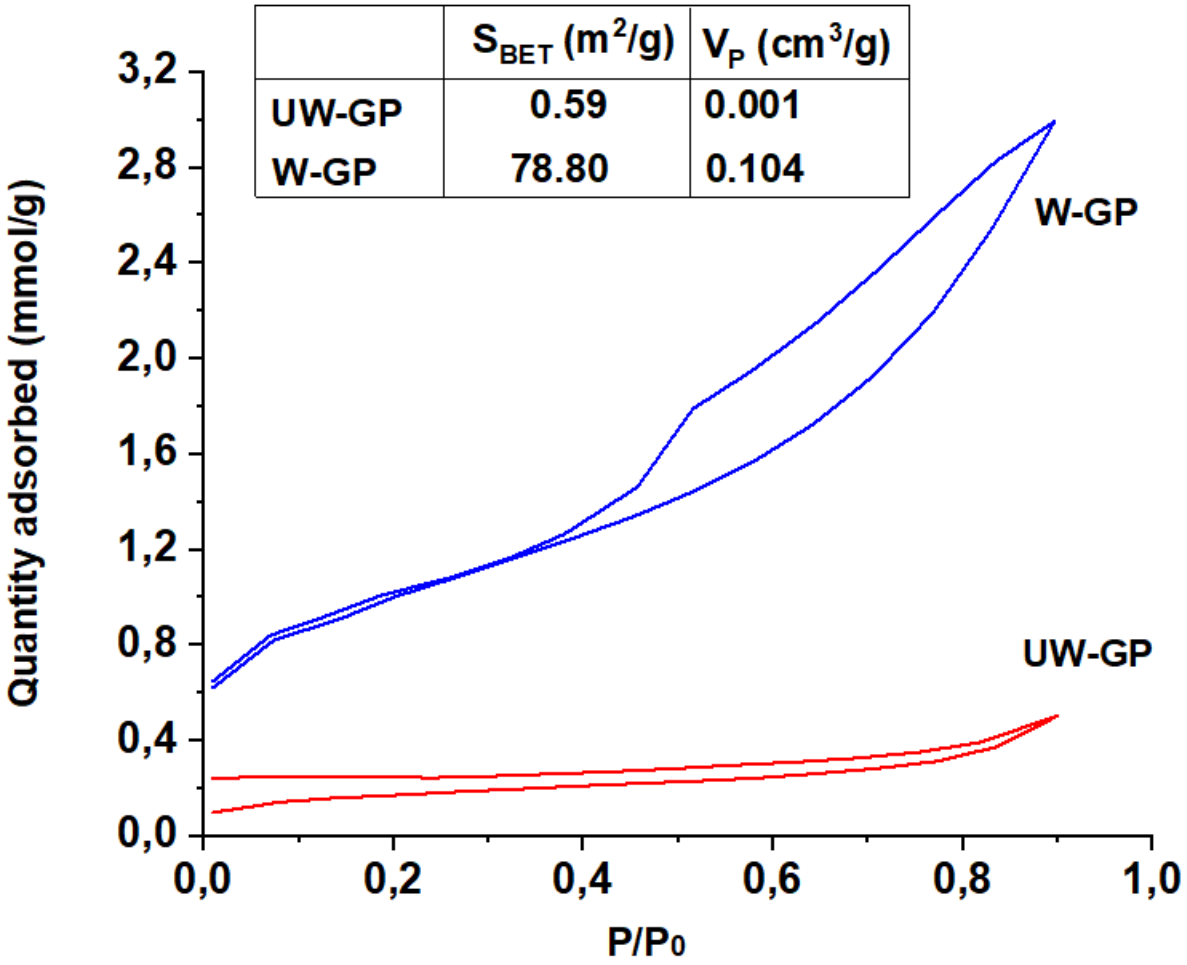

Figure 4

Nitrogen adsorption-desorption isotherms of UW-GP and W-GP.

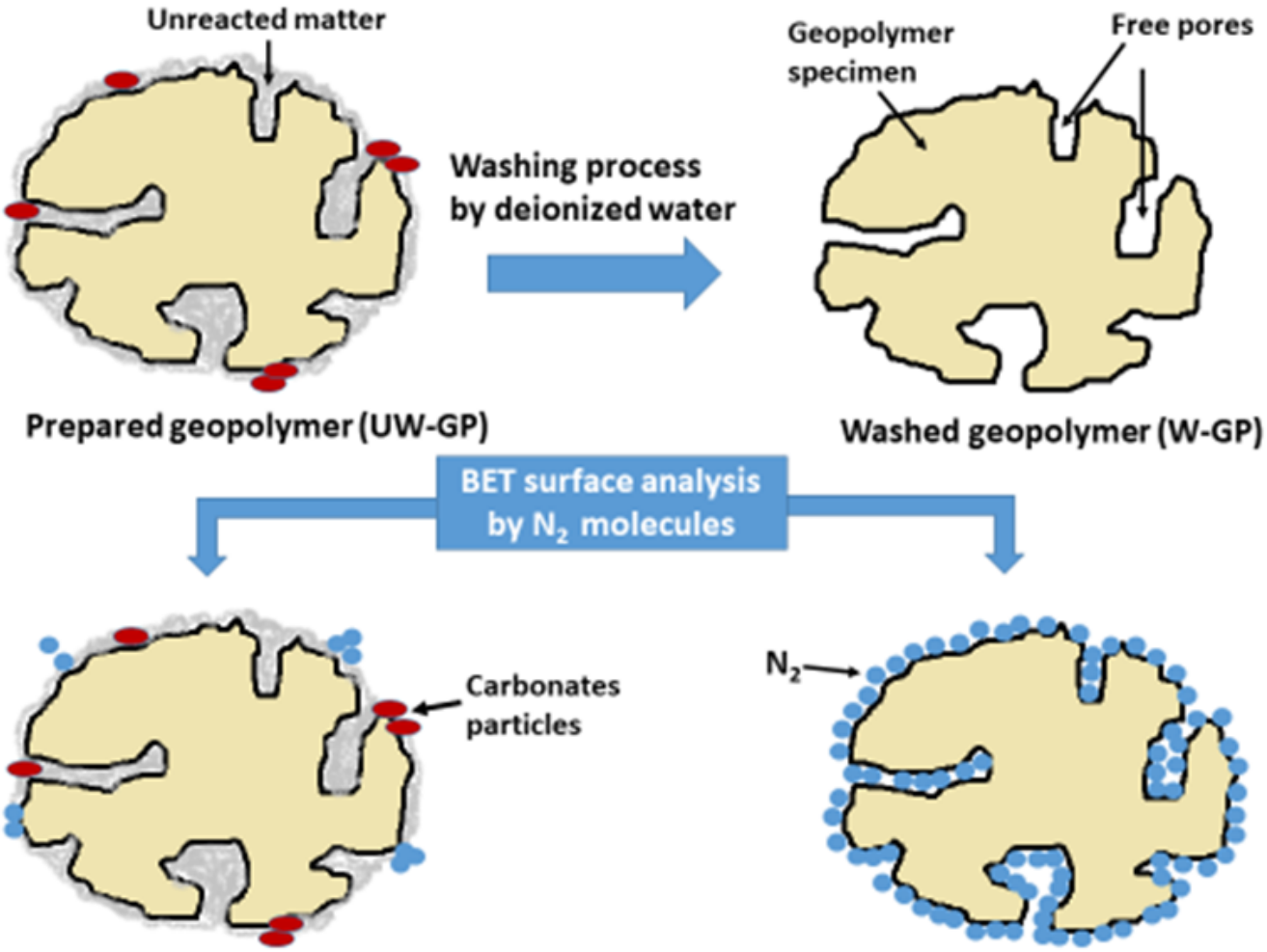

Figure 5

Proposed mechanism shows the interaction of N_2 molecules into washed and unwashed geopolymers surfaces.

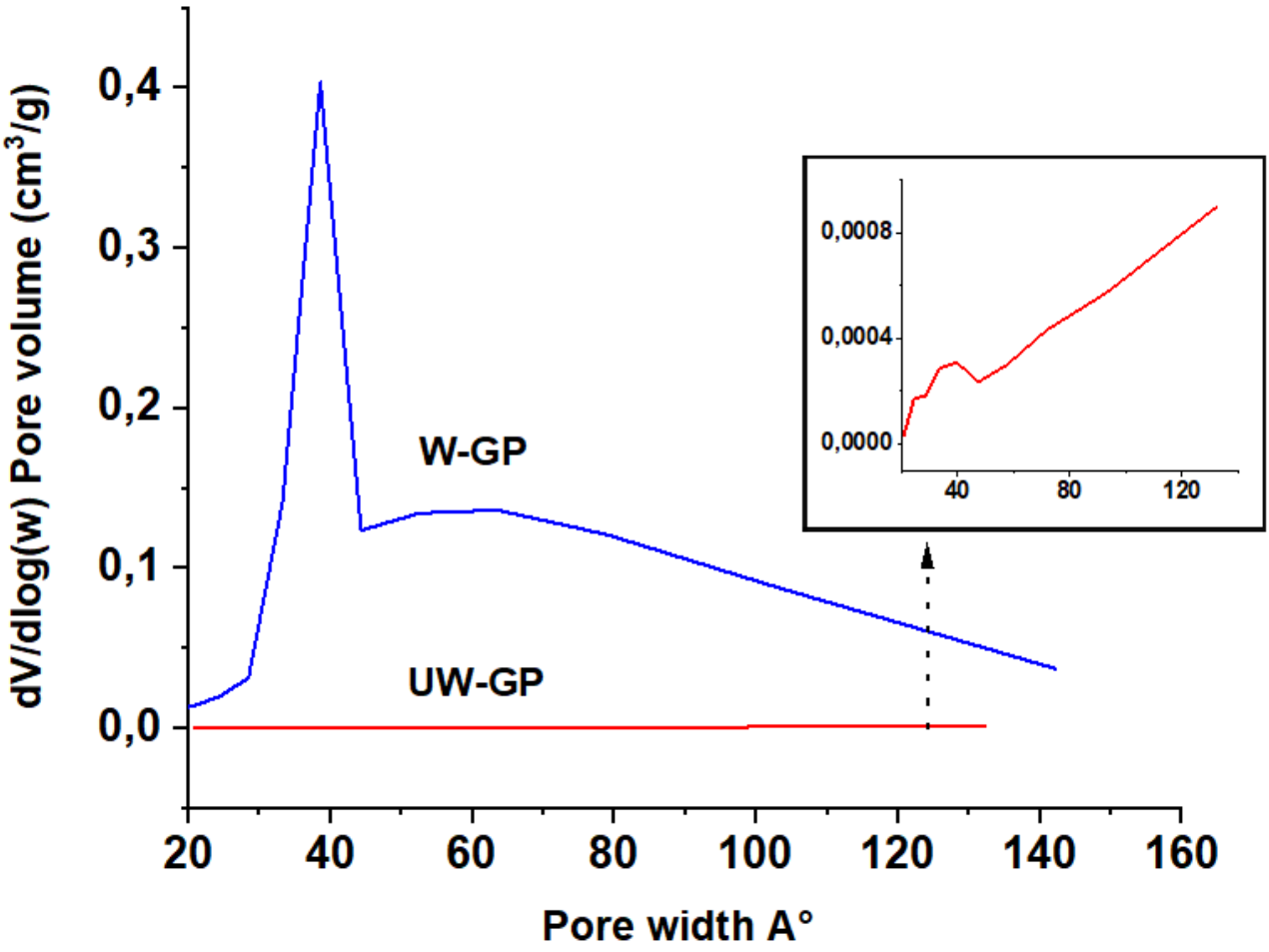

Figure 6

Mesopores width distribution curves determined by BJH method for UW-GP and W-GP.

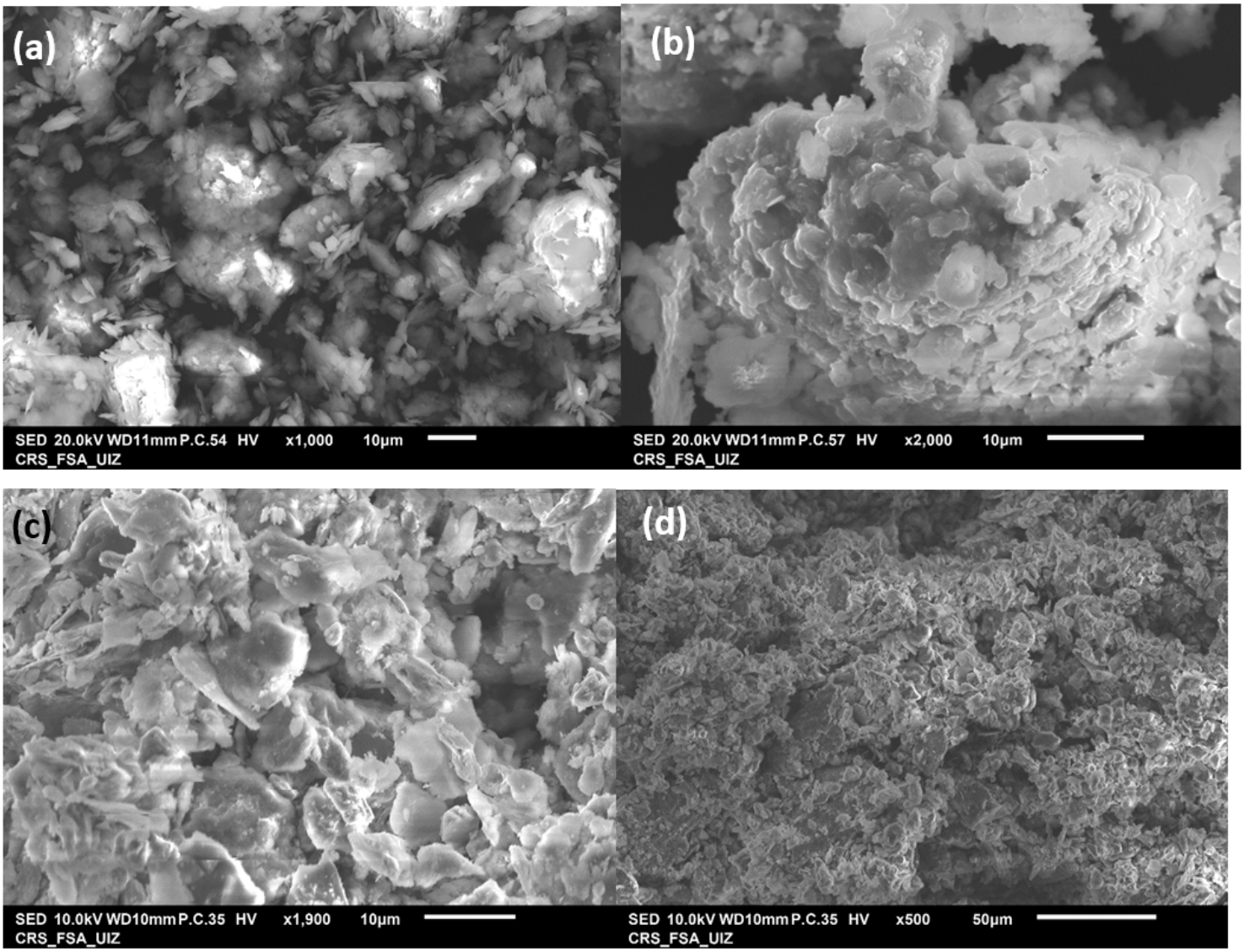

Figure 7

SEM micrographs of metakaolin (a), UW-GP (b) and W-GP (c and d).